KIBRA regulates amyloid β metabolism by controlling extracellular vesicles secretion

Xiaolei Han,[a] Chaoqun Wang,[a] Lin Song,[a,b,c] Xiaojie Wang,[a] Shi Tang,[a,b,c] Tingting Hou,[a,b,c] Cuicui Liu,[a,b,c] Xiaoyan Liang,[a] Chengxuan Qiu,[a,d] Yongxiang Wang,[b,c]* and Yifeng Du [a,b,c]*

[a]Department of Neurology, Shandong Provincial Hospital, Shandong University, No. 324 Jingwuweiqi Road, Jinan, Shandong 250021, PR China
[b]Department of Neurology, Shandong Provincial Hospital Affiliated to Shandong First Medical University, Jinan, Shandong, PR China
[c]Shandong Provincial Clinical Research Center for Neurological Diseases, Jinan, Shandong, PR China
[d]Department of Neurobiology, Care Sciences and Society, Aging Research Center and Center for Alzheimer Research, Karolinska Institutet-Stockholm University, Stockholm, Sweden

Summary

Background Previous research has revealed that KIBRA controls secretion of extracellular vesicles (EVs) by inhibiting the proteasomal degradation of Rab27a and EVs play an important role in amyloid β (Aβ) metabolism and transmission during Alzheimer's disease (AD) pathogenesis. Here, we further test the hypothesis that KIBRA regulates Aβ metabolism *via* the endosomal-lysosomal system.

Methods We generated KIBRA knockout mice on a 5XFAD background and KIBRA knockdown cells in murine HT22 cells with stably overexpressing APP. Various forms of Aβ and quantification of EVs were analyzed by biochemical methods and nanoparticle tracking analysis, respectively. Multivesicular bodies (MVBs) were visualized by electron microscopy and confocal fluorescent microscopy. In a population-based cohort (*n* = 1419), KIBRA genotypes and plasma Aβ levels were analyzed using multiple-PCR amplification and Simoa, respectively.

Findings Multiple forms of Aβ were dramatically attenuated in KIBRA knockout mouse brain, including monomers, oligomers, and extracellular deposition, but KIBRA knockout had no effect on intraneuronal APP C-terminal fragment β (APP-CTFβ)/Aβ levels. KIBRA depletion also decreased APP-CTFβ/Aβ-associated EVs secretion and subsequently enhanced MVBs number. Furthermore, we found that excessive accumulation of MVBs harboring APP-CTFβ/Aβ promoted the MVBs-lysosome fusion for degradation and inhibition of lysosomal function rescued secretion of APP-CTFβ/Aβ-associated EVs. More importantly, whole exon sequencing of KIBRA in a large population-based cohort identified the association of KIBRA rs28421695 polymorphism with plasma Aβ levels.

Interpretation These results demonstrate that KIBRA regulates Aβ metabolism *via* controlling the secretion of APP-CTFβ/Aβ-associated EVs.

Funding National Key R&D Program of China, and National Natural Science Foundation of China.

Keywords: Extracellular vesicles; Lysosomes; KIBRA; Amyloid β; Alzheimer's disease

Introduction

Alzheimer's disease (AD), the most common cause of dementia, is characterized by intracellular accumulation of neurofibrillary tangles and extracellular deposition of amyloid plaques, which are mainly composed of hyperphosphorylated tau protein and peptide amyloid β (Aβ), respectively.[1] Toxic Aβ peptide is generated from the amyloid precursor protein (APP), which undergoes sequential cleavages by β and γ secretases.[2] Although attempts to develop therapies targeting the accumulation of Aβ have not been successful, the amyloid cascade hypothesis is still widely recognized as a plausible explanation of the pathogenesis of AD.[3-5] However, further research is needed to better understand the Aβ

*Corresponding authors at: Department of Neurology, Shandong Provincial Hospital, Shandong University, No. 324 Jingwuweiqi Road, Jinan, Shandong 250021, PR China.

E-mail addresses: wang-yongxiang@hotmail.com (Y. Wang), du-yifeng@hotmail.com (Y. Du).

subcellular metabolism of neurodegenerative disorders such as AD.

It is widely accepted that the homeostasis of APP cleavage and metabolism is critical in the pathogenesis of AD and is related to each organelle of the endolysosomal system, from multivesicular bodies (MVBs) to lysosomes.[6] Under pathological conditions, APP may be internalized into the endosomal-lysosomal system, where APP C-terminal fragment β (APP-CTFβ) and Aβ monomers are generated by β- and γ-secretases, respectively. On one hand, APP-CTFβ/Aβ peptides are sorted to MVBs and eventually release exosomes harboring APP-CTFβ/Aβ into the extracellular space.[7] On the other hand, endocytosed APP and cleaved peptides may also be trafficked to lysosomes for further degradation.[8] Accordingly, the complex APP processing and trafficking network primarily depends on the endosomal-lysosomal-exosomal system, and the impaired balance of endosomal-lysosomal trafficking may lead to abnormal Aβ metabolism, eventually triggering AD pathogenesis. However, the key molecule regulating the balance between lysosomal degradation and exosome secretion is yet largely unknown.

The *WWC1* gene was first described to be associated with human memory performance in a genome-wide search for single nucleotide polymorphisms (SNPs) and the original name, KIBRA, was given for its predominant expression in the KIdney and BRAin.[9] KIBRA is a scaffolding protein enriched at postsynaptic sites,[10] which can interact with various postsynaptic components, including α-amino-3-hydroxyl-5-methyl-4-isoxazolepropionate (AMPA) receptors,[11] actin regulatory networks,[12,13] the atypical protein kinase M ζ,[14] and the synaptic protein dendrin[15] to regulate synaptic plasticity and learning performance. In addition, recent research has demonstrated that the *WWC1* C2 domain has a lipid binding capacity with preference for phosphatidylinositol-3-phosphate (PI3P),[16] which is enriched on endosomal membranes,[17] suggesting that KIBRA may be involved in the regulation of vesicles trafficking in the endolysosomal system. Indeed, our previous research has revealed that KIBRA controls exosome secretion by inhibiting the proteasomal degradation of Rab27a.[18] Given the important role of endosomal-lysosomal-exosomal trafficking in Aβ metabolism, it is reasonable to hypothesize that KIBRA may influence Aβ metabolism by regulating exosome secretion.

In this study, we sought to investigate the role of KIBRA in Aβ metabolism by generating KIBRA knockout mice on a 5XFAD background and KIBRA knockdown cells in murine HT22-APP$_{swe}$ cells. The KIBRA knockout notably decreased APP products from soluble Aβ monomers and oligomers to extracellular plaque deposits in 5XFAD mice. The absence of KIBRA decreased the secretion of extracellular vesicles (EVs) harboring APP-CTFβ/Aβ both *in vitro* and *in vivo*, while increased the accumulation of MVBs in 5XFAD mice. Furthermore, we showed that the colocalization of MVBs with lysosomes and the APP-CTFβ/Aβ degradation through lysosomal pathway was increased in KIBRA knockout mice, and inhibition of lysosomal function rescued extracellular secretion of APP-CTFβ/Aβ-associated EVs. Interestingly, whole exon sequencing of KIBRA from a population-based cohort revealed that only rs28421695 was linked to reduced

concentration of plasma Aβ in older adults. Taken together, our results demonstrated that KIBRA regulates Aβ metabolism by controlling the secretion of EVs carrying APP-CTFβ/Aβ and subsequently increasing lysosomal degradation.

Methods

Animals

5XFAD mice and KIBRA$^{-/-}$ mice were purchased from the Jackson Laboratory (No. 006554 and No. 024415; Bar Harbor, ME, USA). KIBRA was completely knocked out in all tissues of this strain. The 5XFAD mice were crossed with KIBRA$^{-/-}$ mice to generate the KIBRA$^{-/-}$5XFAD and KIBRA$^{+/-}$5XFAD mice. All animal experiments were strictly adhering to ARRIVE guidelines (Animal Research: Reporting of *In Vivo* Experiments). Matched numbers of mice of both sex (males and females) were used in the study. The age, number, and sex of mice used for individual experiments were indicated in the figure legend. All mice were housed under standard conditions with free access to food and water. All efforts were made to reduce the number of animals used and to minimize animal suffering.

Ethics statement

All animal experimental procedures were performed in accordance with the protocols approved by the Institutional Animal Care and Research Advisory Committee of Shandong Provincial Hospital affiliated to Shandong University, Jinan, Shandong, China (NSFC: NO. 2019-058). The study sample of older adults was derived from the ongoing randomized controlled Multimodal INterventions to delay Dementia and disability in China (MIND-China).[19] The protocol of MIND-China was reviewed and approved by the Ethics Committee of Shandong Provincial Hospital in Jinan, Shandong, China (LCYJ: NO. 2018-014). Written informed consent was obtained from all the participants, or in the case of cognitively impaired persons, from a proxy (usually a family member). MIND-China was registered in the Chinese Clinical Trial Registry (registration no.: ChiCTR1800017758).

Reagents and antibodies

The primary antibodies were obtained from the following sources: mouse monoclonal anti-KIBRA (clone 2A5, provided by Prof Jixin Dong's lab), as previously described[18]; mouse monoclonal anti-Alix (Cell Signaling Technology Cat# 2171; Research Resource Identifiers [RRID]: AB_2299455, Danvers, MA, USA; 1:1000 in western blot [WB]); rabbit monoclonal anti-CD63 (Abcam Cat# ab217345; RRID: AB_2754982, Cambridge, UK; 1:1000 in WB and 1:100 in immunofluorescence [IF]); rabbit polyclonal anti-CD63 (Abcam Cat# ab216130, RRID not available; 1:25 in IF); mouse monoclonal anti-APP C1/6.1 C-terminal fragment (CTFs) (Biolegend Cat# 802803, RRID: AB_2715853, San Diego, CA, USA; 1:2000 in WB); rabbit monoclonal anti-BACE1 (Abcam Cat# ab108394, RRID: AB_10861218; 1:1000 in WB); Alexa Fluor 594 anti-4G8 (Biolegend Cat# 800715, RRID: AB_2721291; 1:100 in IF); mouse monoclonal anti-4G8 (Biolegend Cat# 800712, RRID: AB_2734548; 1:400 in IF); mouse monoclonal anti-6E10 (Biolegend Cat# 803004, RRID: AB_2715854; 1:1000 in WB); rabbit polyclonal anti-calnexin (Abcam Cat# ab22595, RRID: AB_2069006; 1:1000 in WB); rabbit monoclonal anti-CD9 (Abcam Cat# ab92726, RRID: AB_10561589; 1:1000 in WB); rabbit monoclonal anti-Cathepsin D (Abcam Cat# ab75852, RRID: AB_1523267; 1:1000 in WB and 1:100 in IF); rabbit monoclonal anti-Rab7 (Abcam Cat# ab137029, RRID: AB_2629474; 1:1000 in WB); rabbit polyclonal anti-oligomer A11 (Thermo Fisher Scientific Cat# AHB0052, RRID: AB_2536236; Waltham, MA, USA; 1:1000 in Dot blots); rat monoclonal anti-LAMP2 (Abcam Cat# ab13524, RRID: AB_2134736; 1:1000 in WB and 1:100 in IF); rabbit monoclonal anti-beta III Tubulin (Abcam Cat# ab18207; RRID: AB_ 444319; 1:300 in IF); rabbit monoclonal anti-NeuN (Abcam Cat# ab177487, RRID: AB_2532109; 1:200 in IF). Bafilomycin A1 (BafA1) (Cat# 88899-55-2, RRID not available) was purchased from MedChemExpress LLC (Monmouth Junction, NJ, USA), and when indicated, the medium contained 20nM BafA1.

Cell culture

Murine HT22 cells were purchased from Guangzhou Jennio Biotech Co. Ltd. (Guangzhou, China) as previously described[18] and were cultured in Dulbecco's modified Eagle's medium (DMEM) (Gibco, Grand Island, NY, USA) supplemented with 10% fetal bovine serum (FBS) (Gibco) and 1% penicillin (100 U/ml), streptomycin (100 μg/ml) (Gibco) in a humidified incubator at 37 °C with 5% CO_2. HT22 cell line was authenticated by species identification and morphological observation and routinely tested for mycoplasma contamination. The HT22 cell line stably overexpressing the human Swedish mutant (K670N, M671L) APP (referred as HT22-APP$_{swe}$ cells) were generated by cloning APP (APP$_{swe}$-mCherry) into the vector CV051-TetIIP-MCS-Ubi-TetR-IRES-Puromycin. Stably overexpressing cells were selected by 3 μg/ml puromycin (P8032, Solarbio Science & Technology Co., Ltd., Beijing, China). The stable cell line was maintained in DMEM with 1 μg/mL puromycin. The APP$_{swe}$ overexpressing cells carry the DOX-inducible Tet-On system and APP$_{swe}$ is induced by 1 μg/ml DOX (GeneChem, Shanghai, China). CRISPR-Cas9 gene-edited KIBRA knockdown and isogenic HT22-APP$_{swe}$ cells (the control cells) were generated by cloning Cas9 vectors and sgRNA targeting the

KIBRA gene into GV393-U6-sgRNA-EF1a-Cas9-FLAG-P2A-EGFP. The sgRNA sequence was as follows: CAT-CAGTGATGAGTTACCGC. After 5−7 days, the KIBRA knockdown cells and their control cells were harvested and designated as KIBRA-KD and CTRL cells, respectively. The LV-Cas9-sgRNA and APP$_{swe}$ overexpression lentiviruses were produced by GeneChem (Shanghai, China).

EVs isolation

2×10^7 cells were cultured in medium supplemented with 10% EVs-depleted FBS (bovine EVs were removed by overnight centrifugation at 100,000 g). After a 48 h incubation in 10 cm culture dish, an equivalent volume of culture medium conditioned by an equivalent number of cells was collected, and the EVs were isolated at 4 °C by sequential centrifugation that strictly adhere to MISEV2018 guidelines.[20,21] Briefly, the medium was centrifuged at 300 g for 10 min to remove dead cells. The supernatants were centrifuged at 2000 g for 10 min and then at 10,000 g for 30 min. The final supernatants were filtered using a 0.22 μm polyvinylidene fluoride (PVDF) membrane filter (Millipore, Billerica, MA, USA) and ultracentrifuged for 70 min at 4 °C and 100,000 g with maximum acceleration and brake using a centrifuge bottle (Cat# 355603, Beckman Coulter, Brea, CA, USA) with a Type 90Ti rotor (k-factor 48, Beckman Coulter). Exosome pellets were washed in phosphate-buffered saline (PBS) and ultracentrifuged at 100,000 g, for 70 min at 4 °C. Finally, pellets were resuspended in PBS or lysis buffer for further WB analysis.

To analyze the effect of KIBRA on EVs secretion *in vivo*, we isolated the extracellular space EVs from the brain of 3−5-month-old mice following MISEV2018 guidelines.[21,22] Freshly removed or previously frozen at −80 °C murine hemi-brain tissue was weighed and transferred to a 15 ml tube, placed in ice water, containing 1.0 mg/ml of collagenase D (11088858001, Roche Diagnostic, Indianapolis, IN, USA) in Hibernate-A (A1247501, Thermo Fisher Scientific Inc., Waltham, MA, USA), at a ratio of 800 μl per 100 mg of brain tissue. The tissue was then incubated in a shaking water bath at 37 °C for a total of 20 min. After incubation, the tissue was immediately returned to ice and a protease inhibitor cocktail (04693132001, Roche Diagnostic) was added to a final concentration 1×. The dissociated tissue was centrifuged following the same sequential centrifugation steps as described above. The washed EVs pellet was resuspended in 2 ml of 0.95 M sucrose solution and inserted inside a sucrose step gradient column (six 2 ml steps starting from 2.0 M sucrose up to 0.25 M sucrose in 0.35 M increments). The sucrose step gradient was centrifuged at 200,000 g with maximum acceleration and brake using a polyallomer ultracentrifuge tube with 13.2 ml capacity (Cat# 344059, Beckman

Coulter) for 16 h at 4 °C (Beckman SW41 Ti, k-factor 124). A total of seven fractions (a-g) were collected, diluted in cold Phosphate-Buffered Saline (PBS), and centrifuged at 100,000 g at 4 °C for 70 min. Seven sucrose gradient fraction pellets were resuspended in 30 μl lysis buffer before further analysis. Fraction d, as the most enriched fraction with EVs (Supplementary Fig. 4), was selected for analysis of the number of released EVs and APP-CTFβ/Aβ content. In addition, the EVs from cell culture supernatants were isolated by the same sucrose step gradient centrifugation as described above before further Aβ analysis.

Gene silencing

KIBRA-KD and CTRL cells were transfected using Lipofectamine 2000 (11668030; Thermo Fisher Scientific, Waltham, MA, USA) with the following small interfering RNAs (siRNAs): control and Rab7 (GenePharma Co., Ltd., Shanghai, China). Then, 24 h after transfection, cells were cultured in EVs-depleted medium for 24 h and EVs were isolated from supernatants as described above. We constructed three siRNA oligo nucleotides and in pilot experiments tested the effects of the three siRNAs on gene silencing prior to the actual experiments. As shown in Supplementary Fig. 7, all sgRNA oligonucleotides against Rab7 had a similar inhibitory effect and the most efficient was chosen for the subsequent experiments. The siRNA sequence was as follows: 5′-GCUGUGUUCUGGUGUUUGATT-3′ and 5′-UCAAACACCAGAACACAGCTT-3′.

Aβ measurements

EVs were isolated from cell culture supernatants and the extracellular space of mouse brain as described above. Cells and EVs were lysed in RIPA buffer (50 mM Tris-HCl pH 8, 150 mM NaCl, 1% Triton X-100, 1% sodium deoxycholate and 0.1% SDS) containing a protease inhibitor cocktail (04693132001, Roche Diagnostic). Levels of Aβ40 and Aβ42 in EVs from the extracellular space of mouse brain were measured using the meso scale discovery (MSD) V-PLEX Aβ Peptide Panel1 (4G8) kit (Meso Scale Diagnostic LLC, Rockville, MD, USA) following the manufacturer's protocol. Levels of Aβ40 and Aβ42 in EVs from cell culture supernatants and cells lysates were measured using a single molecule array (Simoa) platform (Quanterix Corp, MA, USA) with Human Neurology 3-Plex A assay (N3PA), following the manufacturer's instructions.[23]

Mouse hemi-brain was homogenized in 10 volumes of tissue homogenization buffer (50 mM Tris, 150 mM NaCl, 1% Triton X-100, 1% sodium deoxycholate, 0.1% SDS, protease inhibitor cocktail (Roche Diagnostic) to extract soluble β-amyloid. Samples were ultracentrifuged at 100,000 g for 1 h, at 4 °C and supernatants were collected to be used to measure tris-buffered saline

(TBS)-soluble Aβ. The pellet was extracted in 70% formic acid (FA) on ice. Samples were centrifuged at 100,000 g for 1 h at 4 °C and supernatants were collected. FA supernatants were neutralized with 1M Tris-base, pH 11(1:18 v:v) and samples were used to measure FA-soluble Aβ. TBS-soluble and FA-soluble Aβ were measured by sandwich enzyme-linked immunosorbent assay (ELISA) using commercially available kits (27713 for Aβ40 and 27711 for Aβ42, Immuno-Biological Laboratories (IBL), Co., Ltd., Fujioka, Japan) following the manufacturer's protocol. The level of Aβ oligomers was measured using human Aβ oligomers (82E1-specific) Assay Kits (27725, IBL). The level of Aβ42 in cell culture supernatants from KIBRA-KD and their control cells were measured by ELISA kits (27719, IBL). In all cases, samples were measured in duplicates and values were normalized to cell number or brain lysates/weight, respectively.

Immunohistochemistry and image analysis

Following the behavioral tests, the mouse brain tissues were fixed in 4% paraformaldehyde at 4 °C for 24 h, embedded in paraffin and sliced into 5 μm sections or frozen and sliced into 10 μm sections. Coronal paraffin sections were deparaffinized and incubated with 3% H_2O_2 to quench endogenous peroxidases for DAB staining. Antigen retrieval was performed using citrate buffer (0.01 M, pH 6.0, 0.05% Tween-20). The following primary antibodies for coronal paraffin sections were added overnight at 4 °C: anti-4G8 (mouse monoclonal, 1:400, Biolegend Cat# 800712), Alexa Fluor 594 anti-4G8 (1:100, Biolegend Cat# 800715), anti-CD63 (rabbit polyclonal, 1:25, Abcam Cat# ab216130), anti-Cathepsin D (rabbit monoclonal, 1:100, Abcam Cat# ab75852), and anti-LAMP2 (rat monoclonal, 1:100, Abcam Cat# ab13524). The following primary antibodies for coronal frozen sections were added overnight at 4 °C: anti-CD63 (rabbit monoclonal, 1:100, Abcam Cat# ab217345) and anti-LAMP2 (rat monoclonal, 1:100, Abcam Cat# ab13524).

For immunohistochemistry experiments, primary antibodies (anti-4G8, Biolegend Cat# 800712) were detected using ABC HRP kits and developed with DAB (Vector Laboratories, CA, USA) according to the provider's instructions. Sections were imaged using a TissueFAXS plus (TissueGnostics GmbH, Vienna, Austria) and visualized at ×20 magnification using a Zeiss Axio Imager Z2 Microscope System (Carl Zeiss, Jena, Germany). The analysis was quantified using HistoQuest and TissueQuest software (version 6.0.1, TissueGnostics GmbH).

For immunofluorescence experiments, the brain sections were permeabilized with 0.5% Triton-X-100 (Sigma) in PBS and then blocked with 10% bovine serum albumin (BSA, Thermo Fisher Scientific Inc.), and probed with primary antibodies diluted in PBS

overnight at 4 °C. After washing in PBS, the slides were incubated with Alexa Fluor-conjugated secondary antibodies (488 and 594 nm) for 1 h. Coverslips were mounted in ProLong™ Gold Antifade Mountant with DAPI (Thermo Fisher Scientific Inc.). Images of the intracellular APP/Aβ in the cortex and the hippocampus were acquired using a TissueFAXS plus (TissueGnostics GmbH, Vienna, Austria) and visualized at ×20 magnification using a Zeiss Axio Imager Z2 Microscope System (Carl Zeiss, Jena, Germany). The analysis was quantified using HistoQuest and TissueQuest software (version 6.0.1, TissueGnostics GmbH). Confocal images of samples were acquired using a Leica SP5 confocal microscope (Leica Microsystems GmbH, Mannheim, Germany) fitted with a ×63 oil objective and images were processed and assembled using the Leica software. The colocalization analysis was processed with the LAS-AF (Leica Microsystems GmbH) and images were processed with Adobe Photoshop (Adobe Photosystems Inc., San Jose, CA, USA). All analyses were performed in a blinded manner.

Electron microscopy

Anesthetized mice were transcardially perfused with 20 ml of 2% glutaraldehyde and 2.5% paraformaldehyde in 0.1 M PBS at 4 °C to collect the cortical and hippocampal tissues. Then, the cortical and hippocampal tissues were excised immediately and cut into 1 mm³ pieces in cold fixative. Tissue specimens were secondly fixed for 1.5 h with 1% osmium tetroxide in PBS, dehydrated through a graded ethanol series, and embedded in Epon812. Ultrathin sections (70 nm) were prepared, stained with uranyl acetate and lead citrate, and examined by a JEOL-1200EX electron microscope (JEOL, Tokyo, Japan). For quantification of MVBs, MVBs were defined as subcellular organelles containing intraluminal vesicles and monomeric rather than flocculated BSA-gold.

10μl of freshly EVs purified in fraction d from the extracellular space of the mice hemi-brain was absorbed onto carbon-coated formvar Cu grids for 5 min, and then negatively stained with uranyl acetate for 30 s at room temperature. Then the samples were observed immediately at 200 kV with a Talos F200C transmission electron microscopy (Thermo Fisher Scientific Inc., Waltham, MA, USA).

ThS staining

After the sectioned mouse brain tissues were washed three times for 5 min in PBS, the sliced brain tissues were stained with 500 μM of thioflavin S (ThS) solution (MedChemExpress LLC) dissolved in 50% ethanol at room temperature for 8 min. Subsequently, after incubating the tissues twice in 50% ethanol for 3 min, the tissues were washed with PBS for 5 min. Finally, the

stained brain tissue sections were mounted on glass slides using a TissueFAXS plus (TissueGnostics GmbH, Vienna, Austria) and visualized at ×20 magnification using a Zeiss Axio Imager Z2 Microscope System (Carl Zeiss, Jena, Germany). Three brain sections per mouse, each separated by 500 μm, two tissue per brain section were used for quantification. The average of three sections was used to represent a plaque load for each mouse. Analysis of the Aβ plaque in the whole brain, cortex, and the hippocampus was quantified using HistoQuest and TissueQuest software (version 6.0.1, TissueGnostics GmbH). All analyses were performed in a blinded manner.

Immunoblot analysis

Brain tissue samples, cells, and EVs fractions were lysed in RIPA buffer containing a protease inhibitor cocktail (04693132001, Roche Diagnostic). The lysis protein concentration was determined using the colorimetric detection assay (BCA Protein Assay; Pierce, Rockford, IL, USA). For WB analysis, the lysates were normalized by protein concentration, resolved by SDS-polyacrylamide gel electrophoresis (SDS-PAGE), and the proteins were transferred to PVDF membranes (Millipore, Billerica, MA, USA). For Aβ detection, we used the Tricine-SDS-PAGE and the protein were transferred to nitrocellulose membranes (Pall, New York, NY, USA). Exactly 2 μg of brain lysates was spotted for the Dot blots analysis to detect amyloidogenic protein oligomer and Aβ. Membranes were blocked with 5% defatted milk in TBST for 1 h and then incubated with the indicated primary antibodies overnight, followed by detection with HRP-conjugated secondary antibodies and exposure to the Immobilon Western Chemiluminescent HRP substrate (Millipore). The blots were visualized using an Amersham™ image system (GE Health Care, Chicago, IL, USA).

Nanoparticle tracking analysis

The size and concentration of EVs in a given sample were determined through nanoparticle tracking analysis (NTA) on ZetaView platform (Particle Metrix GmbH, Inning am Ammersee, Germany) equipped with a 488 nm laser and a high-sensitivity complementary metal-oxide-semiconductor camera as previously described.[24] Briefly, all samples were diluted in PBS to a final volume of 2 ml. Ideal measurement concentrations were determined by pre-testing the ideal particle per frame value (140−200 particles/frame). For each measurement, two cycles were performed by scanning 11 cell positions. After capture, the videos were analyzed using the in-build ZetaView Software 8.05.05 SP2 with specific analysis parameters: Maximum particle size: 1,000, Minimum particle size 5, Minimum particle brightness: 10.

Quantitative real-time PCR

Total RNA was isolated from cells using the TRIzol reagent (Invitrogen), and complementary DNA was synthesized with the ReverTra Ace qPCR RT Kit (FSQ-101; Toyobo Co., Osaka, Japan). The cDNA was then used to determine the expression levels of the indicated transcripts using a SYBR Green Realtime PCR Master Mix (QPK-201; Toyobo Co.). The following primers were used for the quantitative real-time polymerase chain reaction (qRT-PCR) analyses: 5'-ATCATCCTGGGG-GACTCTGG-3' (forward) and 5'-TCCTTGGTCA-GAAAGTCCGC-3' (reverse) for Rab7; 5'-CACTCTCTGTGAGCTGAACCT-3' (forward) and 5'-GCGGACACACAGGCTACTTT-3' (reverse) for KIBRA; and 5'-GGACACTGAGCAAGAGAGGC-3' (forward) and 5'-TTATGGGGGTCTGGGATGGA-3' (reverse) for GAPDH; GAPDH was used to normalize mRNA expression. Fold changes (FCs) were calculated by the $2^{-\Delta\Delta CT}$ method.

The Morris water maze

The spatial learning and memory abilities of the mice were evaluated using the Morris water maze test, as previously described.[25] In brief, the apparatus included a circular pool with a diameter of 100 cm and a depth of 40 cm filled with water (temperature, 22−24 °C). A platform (8 cm in diameter) was placed at the targeted quadrant at 1.0 cm below the water surface. Four prominent cues were placed outside the maze as spatial references. Mice were placed in the water facing the maze wall at different start positions across trials to search for the platform. If the mice did not find the platform within 60 s, they were guided to the platform where they remained for 20 s. The training lasted for 5 consecutive days, with four sessions per day. The time required to find the hidden escape platform was recorded. The probe trial was performed after 5 days of hidden platform trials. Mice were allowed to swim freely in the water without the platform for 60 s. The frequency of crossing the platform location, the time spent in the platform and target quadrant, and the swimming tracks were monitored.

KIBRA genotype effect on plasma Aβ in humans

The human population sample (n = 1419) was derived from participants in the baseline survey of the MIND-China,[19] a participating project of the World-Wide FIN-GERS Network.[26] AD was diagnosed according to the National Institute of Aging-Alzheimer's Association (NIA-AA) criteria,[27] for probable AD, as previously reported.[28] Multiple-PCR amplification analysis of genomic DNA was performed for participants to detect KIBRA gene Single Nucleotide Polymorphism (SNP) risk loci and exon region.[29] Plasma total-tau, Aβ40, and Aβ42 levels were measured on a Simoa platform

(Quanterix Corp, MA, USA) with Human Neurology 3-Plex A assay (N3PA), following the manufacturer's instructions.[23]

Transfection and constructs

Cells were transfected using Lipofectamine 2000 (11668030; Thermo Fisher Scientific, Waltham, MA, USA) for HT22 cells with overexpressing APP$_{swe}$. The plasmids DsRed-tagged Rab27a chimera were generated by GeneChem (Shanghai, China). Rab27a was amplified and cloned into pDsRed2-N1 plasmids.

Statistical analysis

Data were analyzed using the GraphPad Prism 6.0 software (GraphPad Software Inc., San Diego, CA, USA). Results were expressed as the mean $\pm$ standard error (SE). Technical as well as biological triplicates of each experiment were performed. We used Student's t test to compare differences between two groups and one-way ANOVA analysis to compare difference among multiple groups. The Morris water maze tests were analyzed using two-way ANOVA followed by a Tukey's post hoc test. A two-tailed P value < 0.05 was considered statistically significant. All n and P values and statistical tests are indicated in the figure legends.

Results

KIBRA knockout decreased Aβ pathological burden from monomers, oligomers to extracellular plaques

Previous studies have revealed that APP is cleaved by β-secretase (BACE1) to APP-CTFβ, and further processed by γ-secretase to Aβ40 and Aβ42 monomers, which are then assembled to form soluble Aβ oligomers, and ultimately aggregate to form insoluble amyloid plaque deposits in the brain (Figure 1a).[30] To explore the exact role of KIBRA on Aβ metabolism, multiple antibodies and staining methods were used to specifically identify different forms of Aβ peptides generated from APP metabolism (Figure 1a). We first measured the extracellular insoluble Aβ plaque deposits in the whole brain by ThS staining in KIBRA$^{-/-}$5XFAD mice of different ages. There were significant differences in the area and number of ThS-positive plaques only in younger mice (3−5-month-old), but not in the older mice (>8-month-old) (Supplementary Fig. 1). Consistent with the ThS-staining results (Figure 1b), the levels of FA-soluble Aβ42 but not Aβ40, dramatically decreased in the whole brain of 3−5-month-old KIBRA$^{-/-}$5XFAD mice compared with the 5XFAD mice (Figure 1c), indicating that the depletion of KIBRA in 5XFAD mice significantly reduced the extracellular Aβ deposits in the early stage.

Second, we further investigated the total amyloid burden in the whole brain of KIBRA$^{-/-}$5XFAD mice by the commonly used anti-Aβ monoclonal antibody (4G8), which can recognize various forms of intracellular and extracellular Aβ, including full-length APP, CTFs (CTFα and CTFβ), Aβ monomers, Aβ oligomers, and amyloid plaques (Figure 1a). Compared to 5XFAD mice, 4G8 staining was robustly decreased in KIBRA$^{-/-}$5XFAD mice (Figure 1d), suggesting that KIBRA may regulate APP processing and metabolism. We also investigated the change of soluble Aβ monomers, which is packed into oligomers and dense plaques at the early stages. ELISA analysis revealed that levels of TBS-soluble Aβ42 were significantly decreased in KIBRA$^{-/-}$5XFAD mice, but not for Aβ40 (Figure 1e), which was in line with the levels of Aβ monomers in the whole brain by WB analysis (Figure 1h).

Third, we further investigated whether KIBRA knockout could change the levels of Aβ oligomers, which is believed to be a major cause of neural and synaptic loss due to their high toxicity.[31] Dot blots analysis was performed in the whole brain lysates using anti-amyloidogenic protein oligomer (A11) and 6E10 antibodies, which specifically recognizes oligomeric proteins and full-length APP, APP-CTFβ, and all Aβ species, respectively (Figure 1a). We found that levels of Aβ oligomers were decreased in KIBRA$^{-/-}$5XFAD mice (Figure 1f), which is consistent with levels of 82E1-specific Aβ oligomers detected by ELISA analysis (Figure 1g).

In addition, in order to exclude the possibility that silencing of KIBRA may influence the protein levels of APP and β-secretase, we used the specific APP (C1/6.1) and BACE1 antibody in WB analysis and the results showed that KIBRA knockout markedly decreased the levels of Aβ monomers, oligomers, and APP-CTFs without altering the level of full-length APP and β-secretase (Figure 1i). Taken together, these results demonstrate that depletion of KIBRA in the 5XFAD mice significantly reduced Aβ metabolites from monomers, oligomers to plaque deposits in the early stage, without affecting APP protein level.

KIBRA knockout had no effect on intraneuronal APP-CTFβ/Aβ *in vivo* and *in vitro*

Given that KIBRA depletion led to obvious decrease of total Aβ burden and extracellular amyloid plaque, we further investigated the levels of intraneuronal Aβ in KIBRA$^{-/-}$5XFAD mice. Previous reports have shown that the intraneuronal amyloid burden mainly localized in large pyramidal neurons in cortical layer 5, CA$_1$ and CA$_{2-3}$ pyramidal cells in the hippocampus.[32] Thus, we measured the levels of intraneuronal APP-CTFs/Aβ (4G8 antibody) in cortical large pyramidal neurons and hippocampal region of KIBRA$^{-/-}$5XFAD mice (Figure 2a). Quantitative analysis of 4G8-positive large pyramidal neurons density in the cortex and hippocampal cells (Figure 2b,c) revealed no significant change in
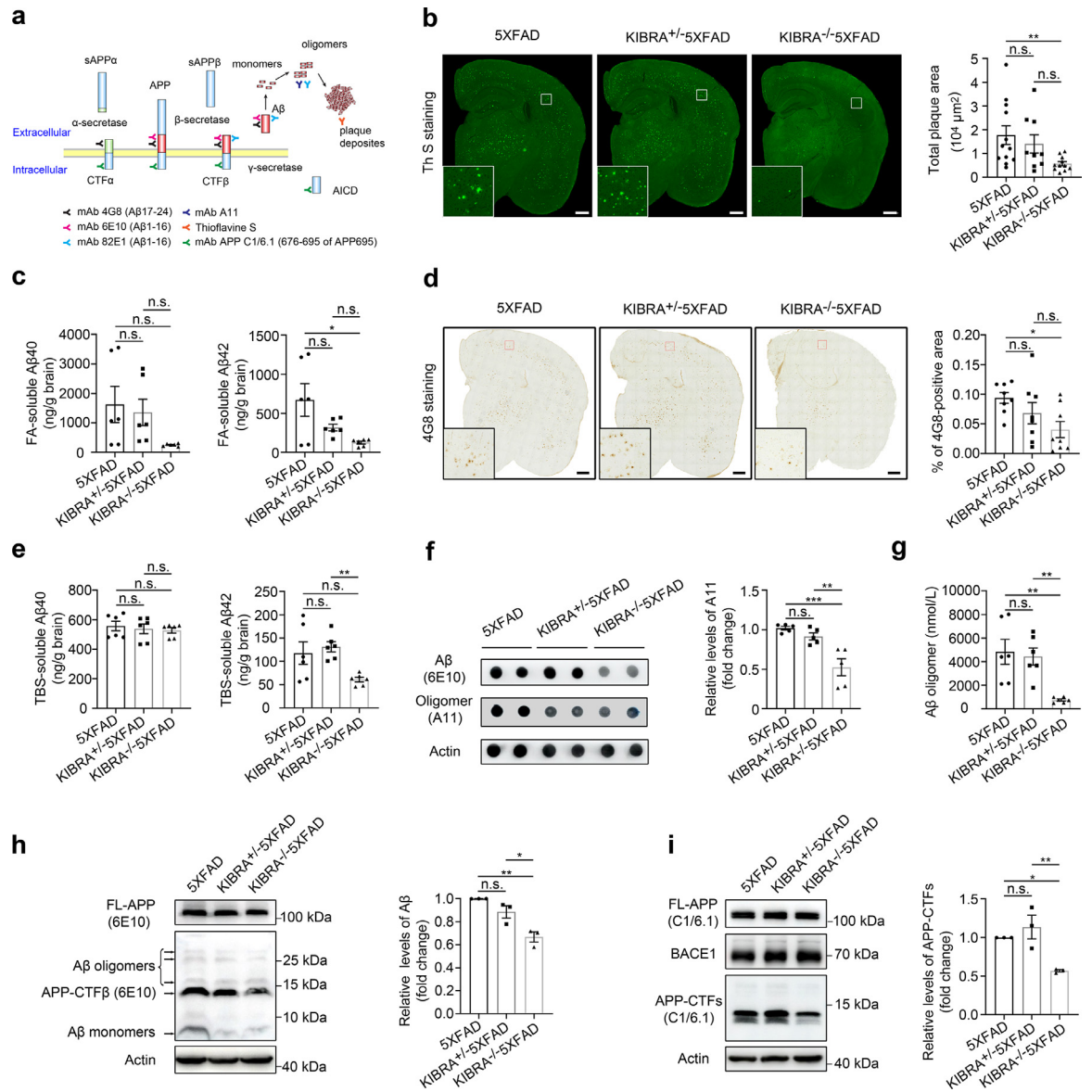
Figure 1. KIBRA Knockout decreases Aβ from monomers, oligomers to extracellular deposits in 5XFAD mice. (**a**) Schematic representation of Aβ-specific antibody recognition sites. (**b**) Representative images and quantification analysis of ThS-stained insoluble Aβ plaques in whole brain of 3−5-month-old mice. Scale bars = 500 μm. 5XFAD (n = 6M/6F), KIBRA$^{+/−}$5XFAD (n = 4M/5F), KIBRA$^{−/−}$5XFAD (n = 6M/5F) mice. (**c**) ELISA analysis of Aβ40 and Aβ42 in formic-acid (FA)-soluble fractions isolated from the whole brain of 3−5-month-old mice. Brain lysates from six mice per group were analyzed. (**d**) Images and quantification analysis of the whole brains from 3−5-month-old mice of corresponding genotypes, labeled with the anti-APP/Aβ antibody (clone 4G8). Scale bar = 500 μm. Eight mice per group were analyzed. (**e**) ELISA analysis of Aβ40 and Aβ42 in TBS-soluble fractions isolated from the whole brain of 3−5-month-old mice. Brain lysates from six mice per group were analyzed. (**f** and **g**) Analysis of Aβ oligomer in the whole brain of the indicated groups. Dot blot analysis of anti-amyloidogenic protein oligomer A11 and quantification analysis of oligomer A11 (**f**), and ELISA analysis of 82E1-specific Aβ oligomers (**g**) from the whole brain lysates of 3−5-month-old mice (n = 6) in the whole brain lysates of the indicated groups. (**h**) WB analysis of brain lysates from indicated 5XFAD mice for full length APP (FL-APP), oligomer Aβ, CTF-β, and Aβ monomer (anti-Aβ: clone 6E10). (**i**) WB analysis of brain lysates from the indicated 5XFAD mice for APP/APP-CTFβ (anti-C1/6.1) and BACE1.Data are represented as the mean ± SE. n.s.≥0.05, $^{***}P < 0.001$, $^{**}P < 0.01$, and $^{*}P < 0.05$ as determined by one-way ANOVA followed by Tukey's post hoc comparisons tests.
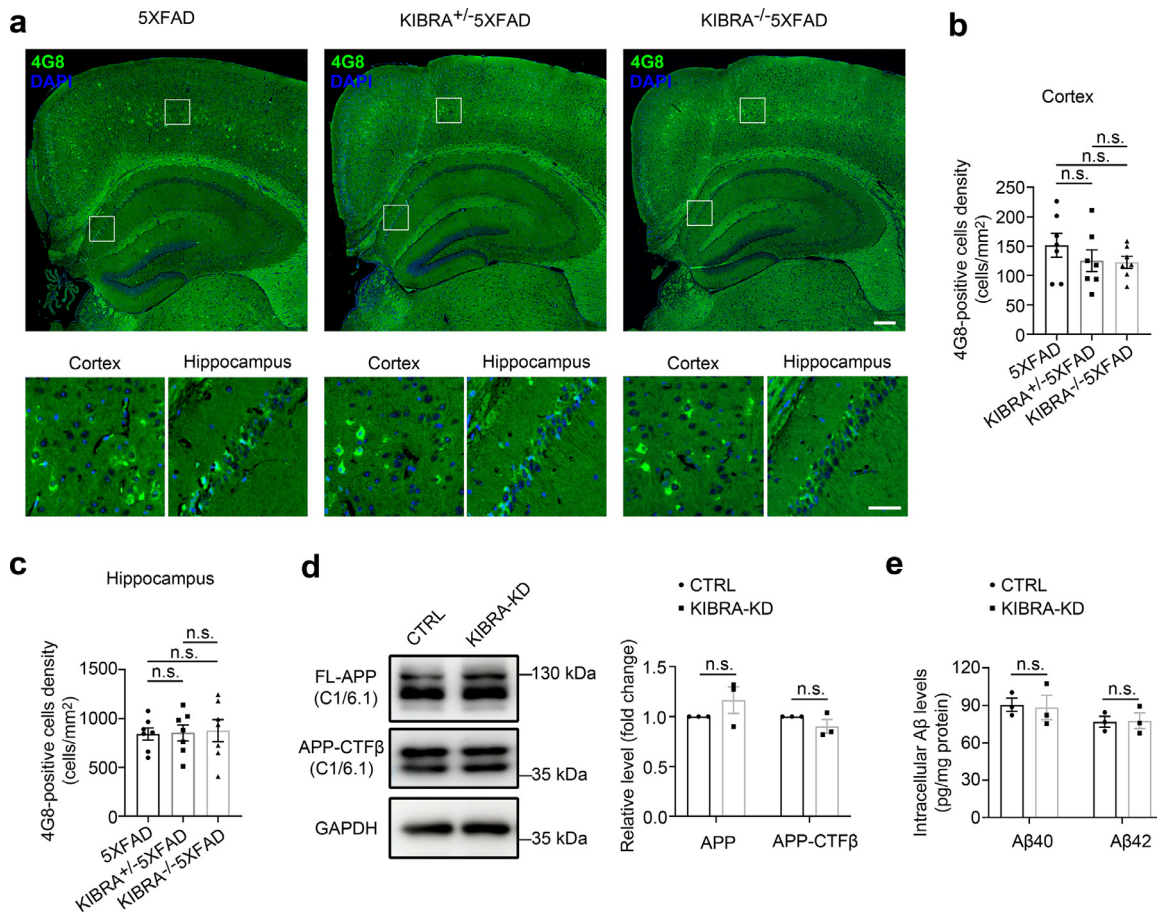
Figure 2. KIBRA Knockout stabilizes intracellular Aβ/AβPP in 5XFAD mice. (**a** and **b**) Representative images and quantification analysis of cortical and hippocampal regions of the indicated 3−5-month-old mice. Intraneuronal Aβ/AβPP in the brain sections were stained with the anti-4G8 antibody (green color), and neuronal nuclear with the DAPI (blue color). Scale bar = 200 μm in upper panel, 50 μm in lower panel. (**b-c**) Quantification analysis of the same cortical (**b**) and hippocampal regions (**c**) of indicated 3−5-month-old mice, respectively. More than seven mice per group were analyzed. (**d**) WB and quantification analysis of cell lysates from the KIBRA-KD and CTRL HT22 cells with APP$_{swe}$ overexpression for APP/APP-CTFβ (anti-C1/6.1). (**e**) Quantification analysis of Aβ40 and Aβ42 levels in cell lysates from the KIBRA-KD and CTRL HT22 cells with APP$_{swe}$ overexpression by Simoa technique. ($n = 3$, from three independent experiments). Data are represented as the mean ± SE. n.s.$\geq$0.05 was determined by one-way ANOVA followed by Tukey's post hoc comparisons tests (**b-c**) or two-tailed Student's t test (**d-e**).

3−5-month-old KIBRA$^{-/-}$5XFAD mice, suggesting that deletion of KIBRA had no effect on intraneuronal APP-CTFs/Aβ *in vivo*. In addition, we silenced KIBRA expression in a mouse hippocampal neuronal cell line (HT22) overexpressing APP$_{swe}$ under the control of doxycycline (DOX). The downregulation of KIBRA was confirmed by both WB analysis and qRT-PCR analysis (Supplementary Fig. 2). Compared with the control cells (CTRL) on a background of overexpressing APP$_{swe}$, intracellular APP and APP-CTFβ levels were unchanged in KIBRA-KD cells (Figure 2d). Intracellular Aβ40 and Aβ42 both displayed no significant difference between CTRL and KIBRA-KD cells by Simoa analysis (Figure 2e); however, Aβ40 or Aβ42 levels in cell culture supernatant of KIBRA-KD cells were decreased (Supplementary Fig. 3), which was consistent with the

results in KIBRA$^{-/-}$5XFAD mice. Taken together, these results demonstrated that KIBRA knockdown had no significant effect on intracellular APP-CTFs/Aβ, only decreases the extracellular APP-CTFs/Aβ.

KIBRA knockout impaired secretion of EVs harboring APP-CTFβ/Aβ

Previous research has demonstrated that MVBs and their contents either are directed to the cell surface where they fuse with the plasma membrane and release the EVs or to the lysosome for degradation.[30] Strikingly, our previous work has shown that KIBRA regulates EVs secretion by inhibiting the proteasomal degradation of Rab27a protein,[18] we next examined whether KIBRA regulates secretion of EVs harboring APP-CTFβ/Aβ.

We generated KIBRA-KD HT22 cells with APP$_{swe}$ over-expression and the EVs were isolated from the conditioned media by both sequential differential centrifugation and sucrose density gradient centrifugation to avoid soluble proteins and protein aggregates contamination for Aβ analysis. The results showed that knockdown of KIBRA led to a significant decrease of EVs biomarker proteins (e.g., Alix, CD63, and CD9) with equivalent numbers of cells, indicating that KIBRA knockdown caused the decrease in the secretion of EVs (Figure 3a,b). In addition, the NTA of the ultracentrifuged pellets revealed a decrease in the number of particles secreted by per KIBRA-KD cell compared with control group (Figure 3c), which was in line with the results by WB analysis. Notably, Aβ40 or Aβ42 peptides (Figure 3d) and APP-CTFβ levels (Figure 3e) in EVs secreted by KIBRA-KD cells showed ∼50% drop compared with equivalent numbers of control cells, demonstrating that depletion of KIBRA decreased the secretion of EVs-associated APP-CTFβ/Aβ in vitro.

To verify the role of KIBRA in exosome secretion in a physiological context, we isolated and purified EVs from the extracellular space of the brains of KIBRA$^{-/-}$5XFAD mice, KIBRA$^{+/-}$5XFAD mice, and 5XFAD mice counterparts by sucrose density gradient centrifugation to avoid the contaminations of soluble proteins and protein aggregates during ultracentrifugation. The contents of the sucrose step gradient fractions (a−g) were analyzed by immunoblotting for proteins known to be either enriched (CD63) or absent (Calnexin) in EVs (Supplementary Fig. 4). Immunoblotting analysis of the sucrose step gradient fractions a to g demonstrated that fraction d was the most enriched with EVs, which was selected for further analysis. To determine whether KIBRA regulates EVs secretion in vivo, the exosomal markers of CD63 and CD9 were quantified in fraction d isolated from the extracellular space of the mouse brain in KIBRA$^{-/-}$5XFAD, KIBRA$^{+/-}$5XFAD, and 5XFAD groups (Figure 3f). Consistent with our previous results,[18] WB analysis showed a decrease of extracellular EVs (CD63 and CD9) in the brain of KIBRA$^{-/-}$5XFAD mice compared to 5XFAD mice (Figure 3g). Notably, Aβ40, Aβ42, and APP-CTFβ levels in the fraction d from the KIBRA$^{-/-}$5XFAD mouse brain displayed significant decrease compared with the 5XFAD mice (Figure 3h,i). In summary, these results demonstrated that downregulation of KIBRA caused a decrease in the secretion of EVs harboring APP-CTFβ/Aβ both in vivo and in vitro.

Since our previous study demonstrated that depletion of KIBRA increased the number of MVBs,[18] we then investigate whether KIBRA regulates Aβ transmission via MVBs to extracellular spaces. As expected, electron microscopy analysis showed that the number of MVBs per cell profiles and intraluminal vesicles (ILVs) per MVB in the hippocampal neurons (Figure 4a) and cortical neurons (Figure 4b) of KIBRA$^{-/-}$5XFAD mice considerably increased compared with the 5XFAD mice, suggesting that KIBRA depletion may lead to excessive accumulation of ILVs and MVBs. In addition, confocal analysis showed that KIBRA knockout significantly increased colocalization of AβPP/Aβ with CD63 in mouse brain neuron (Figure 4c). These findings suggest that deletion of KIBRA may further aggravate the effect of Aβ accumulation by increasing MVBs number.

KIBRA knockout increased APP-CTFβ/Aβ degradation from lysosome

Previous studies have shown that lysosome plays a critical role in protein degradation, especially in Aβ metabolism. We then sought to illustrate the effect of KIBRA knockout with stable expression of mutant APP in mice on lysosome function. Confocal analysis revealed a dramatic increase in the co-localization of CD63 with the lysosome marker Lamp2 in the cortical and hippocampal region of KIBRA$^{-/-}$ mice and KIBRA$^{-/-}$5XFAD mice compared with their control mice, respectively (Figure 5a−c). In addition, immunoblotting analysis indicated that KIBRA knockout markedly increased the expression of lysosomal membrane marker Lamp2 (Figure 5d,e). Considering that measuring lysosomal hydrolases is critical to monitor lysosomal degradation function, we used WB analysis to measure the maturation of cathepsin D (Cat D), a lysosomal hydrolase produced as precursor proCatD (∼50 kDa) and sorted to the endolysosomal compartment, where it is processed into a mature form (∼30kDa) at acidic pH.[33,34] We found that CatD/proCatD ratio was increased in KIBRA$^{-/-}$5XFAD mice, compared with 5XFAD mice in both cortical and hippocampal regions in vivo (Figure 5d,e). In addition, we found that the maturation of Cat D was also increased in KIBRA-KD HT22-APP$_{swe}$ cells in vitro (Supplementary Fig. 5), based on the increased CatD/proCatD ratio, but not in total levels. Furthermore, there was significantly more co-localization of AβPP/Aβ (stained by antibody 4G8) and lysosomal marker Lamp2 in the cortical pyramidal neurons of 3−5-month-old KIBRA$^{-/-}$5XFAD mice (Figure 5f), and KIBRA knockout showed increased colocalization of AβPP/Aβ with Cat D in neurons (Figure 5g). These findings support the view that KIBRA knockout indirectly increases colocalization of MVB CD63 marker with lysosomal LAMP2 marker and facilitates the APP-CTFβ/Aβ degradation by lysosomes.

Inhibition of lysosomal function rescued secretion of EVs harboring APP-CTFβ/Aβ

To determine whether inhibition of lysosomal function rescued the release of EVs enriched for APP-CTFβ/Aβ, we treated KIBRA KD cells and its corresponding control cells with the lysosome inhibitor BafA1, which specifically inhibits the proton pump, increases the pH of
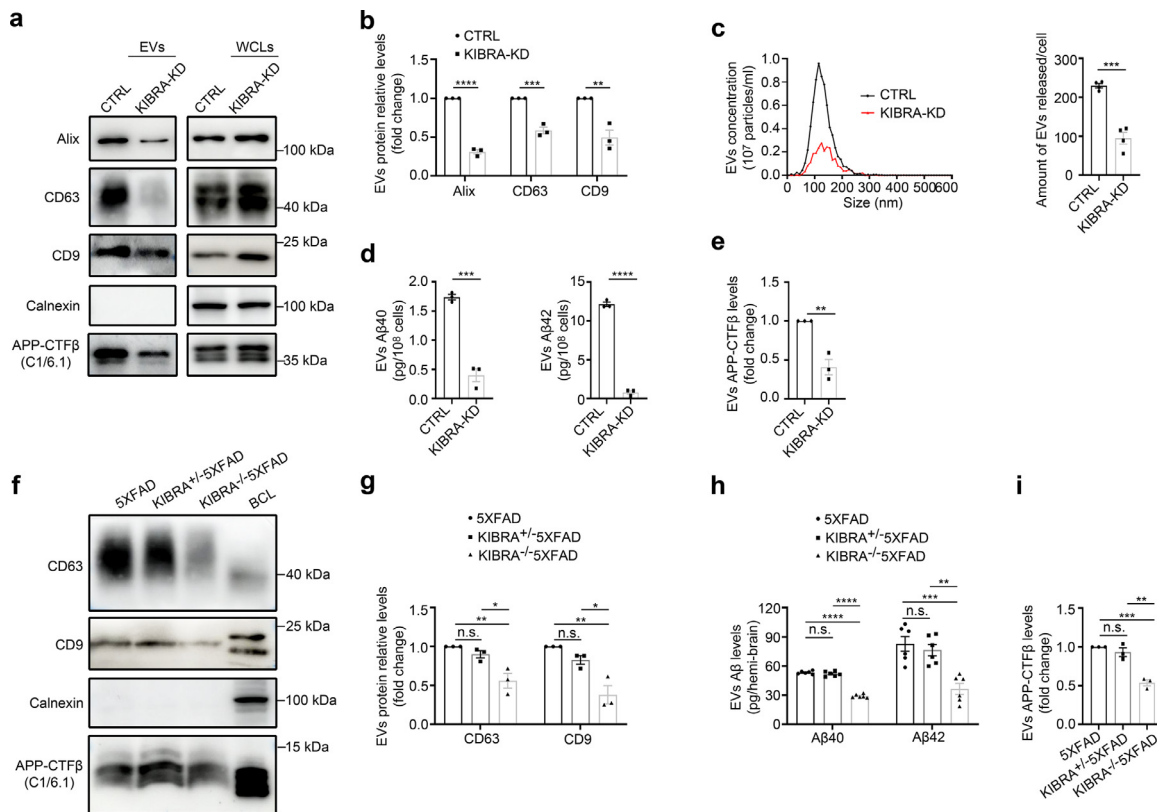
Figure 3. KIBRA Knockout reduces secretion of EVs harboring APP-CTFβ/Aβ both *in vivo* and *in vitro*. (**a**) WB analysis of small EVs from cell culture supernatants from equal number of KIBRA-KD and CTRL HT22 cells overexpressing APP$_{swe}$. Whole cell lysates (WCLs) and small EVs were blotted for the EVs markers Alix, CD63, CD9, and APP-CTFβ and for the endoplasmic reticulum marker Calnexin. (**b**) Quantification of EVs protein levels in the small EVs obtained from KIBRA-KD and CTRL cells overexpressing APP$_{swe}$ in three independent experiments. (**c**) Representative NTA traces of EVs isolated from cell culture supernatants from equal numbers of KIBRA-KD and CTRL cells overexpressing APP$_{swe}$. Quantification of NTA of four independent experiments. (**d**) Simoa analysis was used to measure human Aβ40 and Aβ42 levels in small EVs purified from sucrose step gradient centrifugation from equal numbers of KIBRA-KD and CTRL cells with APP$_{swe}$ overexpression. (n = 3, from three independent experiments). (**e**) Quantification of exosomal APP-CTFβ levels in the small EVs obtained from KIBRA-KD and CTRL cells overexpressing APP$_{swe}$ in three independent experiments. (**f**) Sucrose step gradient fraction d isolated from the extracellular space of the brain from 3−5-month-old of the indicated groups mice were blotted for the exosomal markers CD63, CD9, Calnexin, and APP-CTFβ. (**g**) Quantification of exosomal protein levels in the small EVs obtained from the indicated groups mice in three independent experiments. (**h**) Human Aβ40 and Aβ42 levels were measured by MSD analysis from sucrose step gradient fraction d isolated from the extracellular space of the brain from 3−5-month-old indicated groups mice (n = 6, from three biological replicates). (**i**) Quantification of exosomal APP-CTFβ levels in the small EVs obtained from the indicated groups mice in three independent experiments. Data are represented as the mean $\pm$ SE. In **a-e**, $^{**}P < 0.01$, $^{***}P < 0.001$, and $^{****}P < 0.0001$ in two-tailed Student's t test. In **f-h**, $^*P < 0.05$, $^{**}P < 0.01$, $^{***}P < 0.001$, and $^{****}P < 0.0001$ as determined by one-way ANOVA followed by Tukey's post hoc comparisons tests.

lysosomes, and leads to the dysfunction of cathepsin D in lysosomes (Supplementary Fig. 6) and inhibits trafficking between MVB and lysosomes.[35,36] After BafA1 treatment for 12 h, the number of released EVs was dramatically increased in KIBRA KD cells (second v.s. last column, Figure 6b), indicating that the effect of inhibition of lysosomes function partially rescues decrease of EVs secretion from KIBRA depletion. In addition, exosomal protein levels remarkably increased in KIBRA KD cells after treatment with BafA1 (second v.s. last column, Figure 6d,e), which was consistent with the NTA analysis results. Furthermore, Aβ40, Aβ42 peptides

(Figure 6c), and APP-CTFβ (Figure 6f) in EVs were also remarkably increased in KIBRA KD cells after BafA1 treatment. These findings suggest that inhibition of lysosomal function partially rescues secretion of EVs-associated APP-CTFβ/Aβ from KIBRA depletion.

To exclude the non-specific effects of lysosome inhibitor on the fusion of MVBs to lysosomes, we knocked down the expression of Rab7 using siRNA technology (Supplementary Fig. 7), which is reported to primarily mediate MVB-lysosome fusion.[37] Our results showed that Rab7 knockdown rescued EVs secretion in KIBRA KD cells (second v.s. last column, Figure 6h,i),
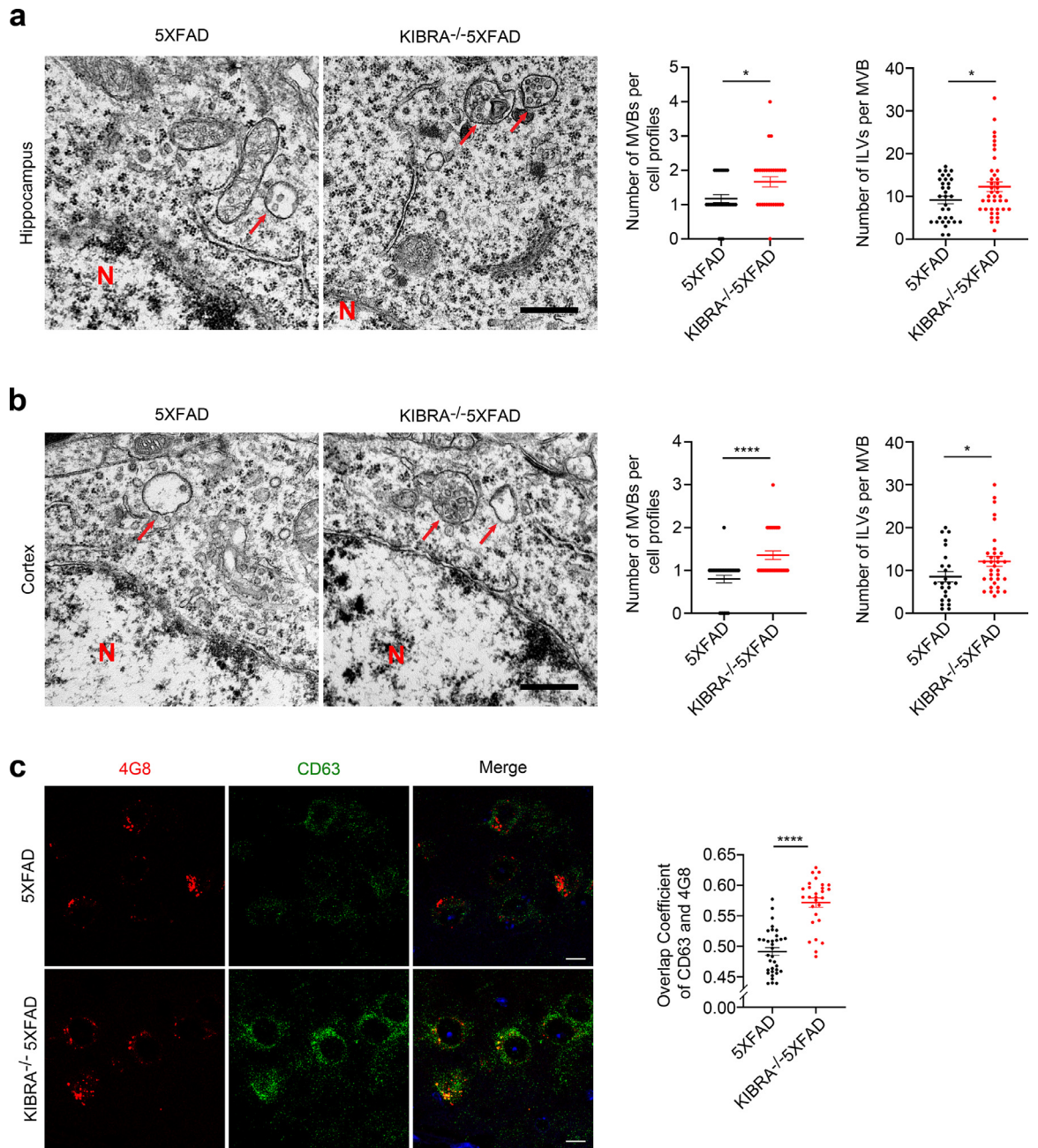
Figure 4. KIBRA knockout causes increases in number of MVBs harboring AβPP/Aβ. (**a** and **b**) Representative electron microscopic images of the hippocampus (**a**) and cortex (**b**) area in KIBRA$^{-/-}$5XFAD and 5XFAD mice. Scale bar = 500 nm. Red arrows indicate MVBs containing typical ILVs. Quantification analysis of the number of MVBs per cell profile and the number of ILVs per MVB. ILVs and MVBs in 28-31 profiles of different cells were counted in a blind manner and only MVBs containing typical ILVs were counted. (**c**) Confocal microscopy analysis of Aβ/AβPP (anti-Aβ, clone 4G8, red) with CD63 (green) in brain slices of KIBRA$^{-/-}$5XFAD and 5XFAD mice. Scale bar = 10 μm. Right panel represents overlap coefficient per cell. Data are represented as the mean ± SE. *$P < 0.05$, ***$P < 0.001$, and ****$P < 0.0001$ in two-tailed Student's t test.

supporting the notion that inhibiting the fusion of excessive MVBs to lysosomes rescued EVs secretion from KIBRA depletion. Consistent with the exosomal marker change, the NTA analysis revealed that the number of released EVs was also dramatically increased after knocking down Rab7 in KIBRA KD cells (Figure 6k). More importantly, the APP-CTFβ level (Figure 6j, second column v.s. last column) and the levels of Aβ40 and Aβ42 peptides (Figure 6l, second column v.s. last column) in the EVs were
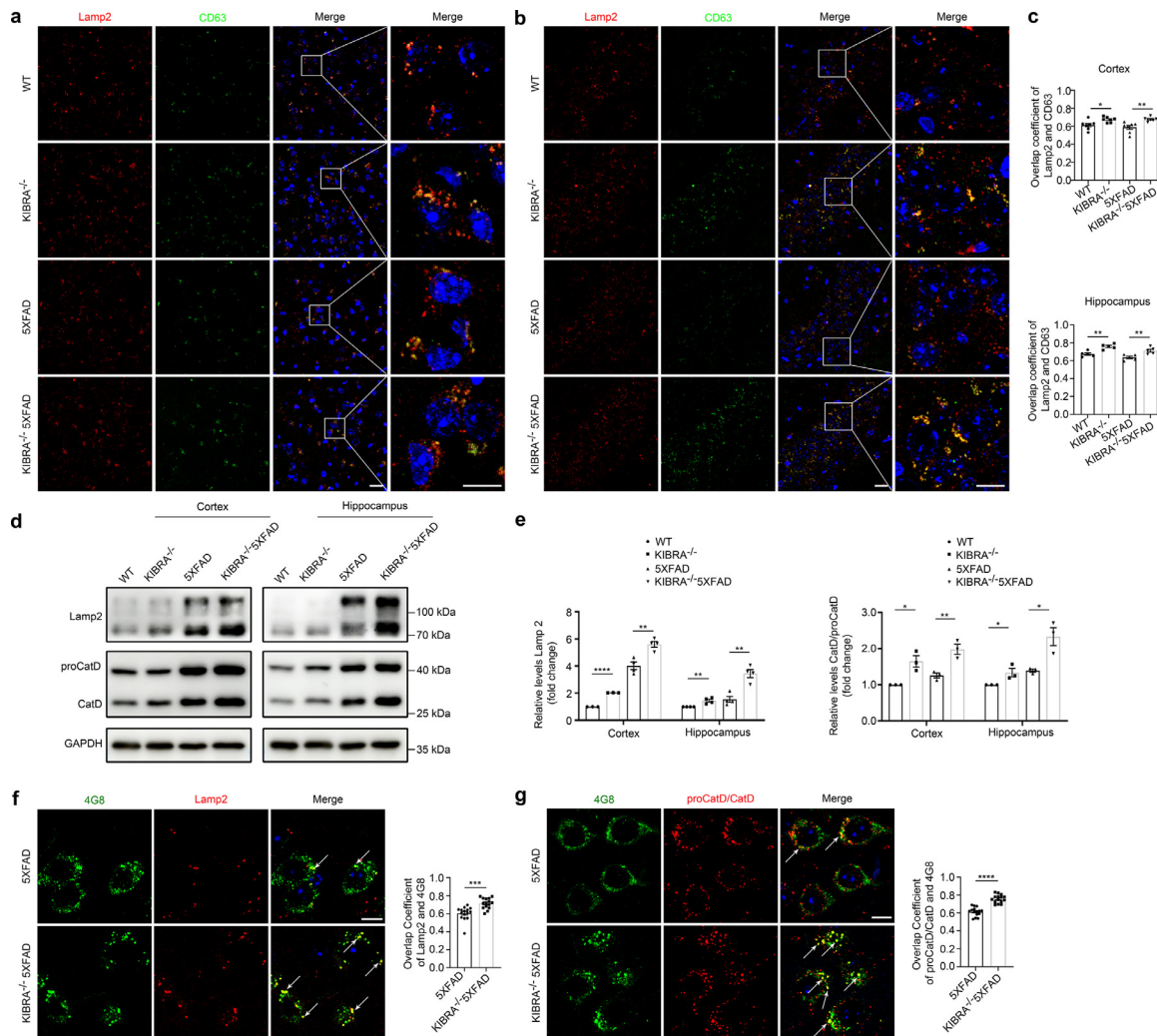
Figure 5. KIBRA Knockout leads to AβPP/Aβ aggregation and degradation by lysosomes. (**a** and **b**) Confocal microscopy analysis of MVBs marker CD63 (green) and lysosomal marker LAMP2 (red) co-localization in cortical layers 5 (**a**) and hippocampal CA_{1-3} (**b**) regions of WT, KIBRA$^{-/-}$, 5XFAD, and KIBRA$^{-/-}$5XFAD mice. Nuclei were stained with DAPI. Scale bar in left panel = 20 μm. Scale bar in right panel = 10 μm. (**c**) Quantification analysis of overlap coefficient per view ($n = 7$ in the cortex and $n = 5$ in the hippocampus). (**d**) WB analysis of lysosomal marker Lamp2 and Cathepsin D levels in brain tissue lysates from cortical and hippocampal regions of 3−5-month-old mice. (**e**) Quantification analysis of lysosomal membrane protein levels (Lamp2, left panel) and ratio of CatD/pro-CatD (right panel) in cortical and hippocampal regions from 3−5-month-old mice of the indicated genotypes. Quantification results were plotted as dot plots, showing the mean ± SE of at least three independent experiments. *$P < 0.05$, **$P < 0.01$, ****$P < 0.0001$ as determined by a two-tailed t test. (**f**) Confocal microscopy analysis of lysosomal membrane marker Lamp2 (red) with Aβ/AβPP (anti-Aβ, clone 4G8, green) in brain slice of 5XFAD and KIBRA$^{-/-}$5XFAD mice. Scale bar = 10 μm. The overlap coefficient per cell was quantified ($n = 15$). (**g**) Confocal microscopy analysis of Cathepsin D (red) with Aβ/AβPP (anti-Aβ, clone 4G8, green) in brain slice of 5XFAD and KIBRA$^{-/-}$5XFAD mice. Scale bar = 10 μm. Overlap coefficient per cell was quantified ($n = 15$). **f-g**. Quantification result were plotted as dot plots, showing the mean ± SE. ***$P < 0.001$, ****$P < 0.0001$ as determined by a two-tailed student's t test.

significantly increased in KIBRA KD cells after treatment with siRNA targeting Rab7. These findings suggest that KIBRA regulates Aβ metabolism mainly by controlling secretion of EVs-associated APP-CTFβ/Aβ, and inhibiting the fusion of excessive MVBs to lysosomes rescued EVs-harboring APP-CTFβ/Aβ secretion.

KIBRA genotype was associated with plasma Aβ levels in humans

To explore whether KIBRA gene SNPs are associated with plasma Aβ levels in human population, we sequenced whole exons of KIBRA on chromosome 5q34 in the subsample derived from the MIND-China study ($n = 1419$). In nine missense mutations (SNPs)
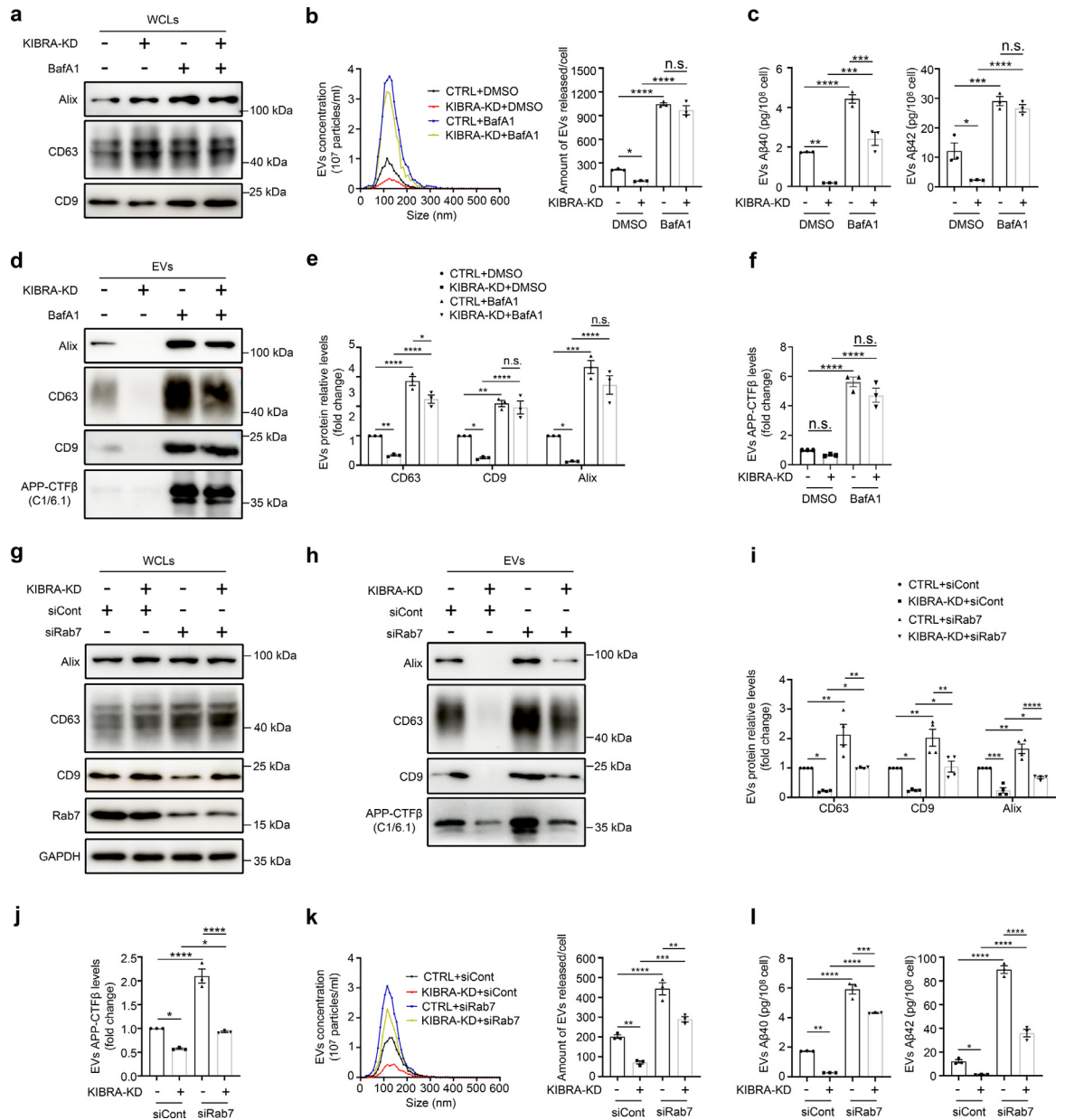
Figure 6. Inhibition of lysosome function in KIBRA knockout cells rescues secretion of EVs harboring APP-CTFβ/Aβ. (**a**) WB analysis of WCLs in KIBRA-KD and CTRL cells overexpressing APP_swe, and treated with 20 nM bafilomycinA1 (BafA1) for 12 h, when indicated, and WCLs were blotted for Alix, CD63, and CD9. (**b**) Representative NTA traces of EVs derived from KIBRA-KD and CTRL cells overexpressing APP_swe, and treated with BafA1. Right panel represents quantification of NTA of three independent experiments. (**c**) Human Aβ40 and Aβ42 levels measured by Simoa analysis from small EVs purified from sucrose step gradient centrifugation from equal number of KIBRA-KD and CTRL cells overexpressing APP_swe, and treated with BafA1. ($n = 3$, from three independent experiments). (**d**) WB analysis of EVs secretion in KIBRA-KD and CTRL cells overexpressing APP_swe, and treated with 20 nM bafilomycinA1 (BafA1) for 12 h, when indicated. EVs were blotted for Alix, CD63, CD9, and APP-CTFβ. (**e**) Quantification of EVs protein levels in the small EVs obtained from KIBRA-KD and CTRL cells overexpressing APP_swe, and treated with lysosome inhibitor BafA1 in three independent experiments. (**f**) Quantification of APP-CTFβ levels in the small EVs obtained from KIBRA-KD and CTRL cells overexpressing APP_swe, and treated with lysosome inhibitor BafA1 in three independent experiments. (**g** and **h**) WB analysis of EVs secretion in KIBRA-KD and CTRL cells overexpressing APP_swe transfected with control small interfering RNAs (siRNAs) or siRNAs targeting Rab7. WCLs (**g**) and EVs (**h**) were blotted for Alix, CD63, CD9, Rab7, and APP-CTFβ. (**i**) Quantification of EVs protein levels (Alix, CD63, and CD9) in the small EVs obtained from KIBRA-KD and CTRL cells overexpressing APP_swe, and transfected with siRNAs in four independent experiments. (**j**) Quantification of APP-CTFβ levels in the small EVs obtained from KIBRA-KD and CTRL cells overexpressing APP_swe,

identified within the KIBRA coding region (Figure 7a), only one of these SNPs (rs28421695) was significantly associated with plasma Aβ40 level ($P < 0.0001$, two-tailed student's t test) and marginally associated with plasma Aβ42 level ($P = 0.0889$, two-tailed student's t test). The results showed that plasma concentrations of Aβ40 in subjects with T-allele of rs28421695 (A/T) were dramatically lower compared to subjects with A/A (Figure 7b) and Aβ42 in subjects with T-allele of rs28421695 (A/T) were marginally lower compared to subjects with A/A (Figure 7c), while the Aβ42/Aβ40 ratio was significantly higher in persons with A/T compared to those with A/A (Figure 7d). The rs28421695 polymorphism resides on exon Glu-rich domain in the KIBRA locus,[38] and the T-variant of this allele results in E862V substitution (Figure 7a). These results demonstrate that KIBRA SNP rs28421695 was significantly associated with reduced plasma Aβ levels in humans, which may correlate the loss of function of KIBRA with lower EVs secretion and Aβ metabolites.

Discussion

The current study is based on our previous work, which shows that KIBRA depletion dramatically decreases EVs secretion, which is accompanied by down-regulation of the Rab27a protein, a small GTPase reported to regulate MVB docking to the plasma membrane.[18] In the current study, we sought to further explore the effect of KIBRA on Aβ metabolism by generating KIBRA knockout mice on a 5XFAD background. We found that KIBRA knockout significantly ameliorated extracellular Aβ deposits at early stage of the disease, which was attributed to KIBRA, primarily by controlling secretion of EVs-associated APP-CTFβ/Aβ and subsequently increasing the excessive MVB-lysosome fusion for amyloid degradation. In addition, we identified a KIBRA SNP, rs28421695, which was associated with reduced level of plasma Aβ in humans.

Endosomal sorting and trafficking dysfunction is one of the earliest cellular feature of AD and all the organelles of the endolysosomal system, from MVBs to lysosomes, contribute to the homeostasis of APP cleavage products, including all Aβ peptides.[6,30,39] In this study, we found that the numbers of MVBs and ILVs were higher in KIBRA$^{-/-}$5XFAD mice compared with the control 5XFAD mice, which was in line with the dramatic increase in the number of MVBs in neurons of KIBRA knockout mice,[18] and Aβ accumulation also causes MVB enlargement.[40] Studies conducted by

Rajendran et al. found that Aβ produced in the early endosome was transported to MVBs and packaged into EVs for secretion.[41] Our study clearly showed that APP/Aβ clearly colocalized with CD63-positive MVBs (Figure 4c), which is in line with the previous reports.[40–42] In addition, accumulation of aggregation-prone Aβ42 is strongly likely to localize in intracellular acidic compartments (e.g., late endosomes and lysosomes) in cells expressing FAD-causing mutations.[43]

A key finding reported in this study is that depletion of KIBRA leads to ameliorate the extracellular amyloid deposits at early stage rather than late stage of the disease in AD mouse model, which could be explained by the fact that excessive amyloid accumulation in neurons and brain aging in older mice may induce chronic accumulation of dysfunctional lysosomes,[44,45] and result in failed degradation of misfolded proteins in neurons. Intriguingly, we did not find significant difference in learning and memory function between KIBRA knockout mice and the controls in a 5XFAD background (Supplementary Fig. 9), but the neuronal density was higher in KIBRA$^{-/-}$5XFAD mice (Supplementary Fig. 10). However, we found that compared to WT mouse, KIBRA deficiency resulted in impaired cognitive performance, which is consistent with a recent report demonstrating that KIBRA modulates learning and memory by binding to dendrin or stabilizing protein kinase Mζ.[14,15] Our previous study also confirmed that KIBRA exerted a neuroprotective function by promoting neuronal survival in vitro.[46] Therefore, KIBRA, as a multifunctional scaffold protein with around 20 known binding partners,[38] may be linked to distinct or even converse functions in cognitive phenotypes, neuron survival, and Aβ metabolism depending on various cell types and pathophysiological environments.

Another important finding in our study is that KIBRA deletion causes a reduction of the EVs-associated APP-CTFβ/Aβ both in vivo and in vitro. EVs are increasingly involved in the transmission and aggregation of misfolded proteins (e.g., Aβ, tau, and α-synuclein).[47–50] However, little is known about the physiological mechanisms regulating misfolded proteins propagation and aggregation.[42] Recent studies have shown that circulating EVs-bound Aβ peptides significantly reflect PET imaging of brain amyloid plaques,[51] and EVs reduction in vivo is associated with a lower amyloid plaque load in 5XFAD mice.[52,53] These reports revealed that EVs may work as nucleation centers for the aggregation of Aβ into fibers. In support of this hypothesis, it was found that apolipoprotein E in

and transfected with siRNAs in three independent experiments. (**k**) Representative NTA traces of EVs derived from KIBRA-KD and CTRL cells overexpressing APP$_{swe}$, and treated with siRNAs targeting Rab7. Right panel represents quantification of NTA of three independent experiments. (**l**) Human Aβ40 and Aβ42 levels measured by Simoa analysis from small EVs purified from sucrose step gradient centrifugation from equal numbers of KIBRA-KD and CTRL cells overexpressing APP$_{swe}$, and treated with siRNAs in three independent experiments. The quantification results were plotted as dot plots, showing the mean $\pm$ SE. *$P < 0.05$, **$P < 0.01$, ***$P < 0.001$, ****$P < 0.0001$, n.s., not significant ($P > 0.05$) as determined by one-way ANOVA followed by Tukey's post hoc comparisons tests.

a

Position	SNP	m/M	AAS	MAF	Plasma Aβ40, pg/mL			Plasma Aβ42, pg/mL		
					MM	Mm/(mm+Mm)	P value	MM	Mm/(mm+Mm)	P value
167881032	rs28421695	T/A	E862V	0.0530	180.82	161.88	**<0.0001**	12.01	11.55	**0.0889**
167835539	rs17551608	T/C	R250C	0.0068	179.28	159.21	0.0612	11.97	11.43	0.4369
167855044	rs61730019	G/A	N606S	0.0004	178.90	326.17	-	11.96	14.44	-
167855743	rs79212989	G/A	S651G	0.0335	178.63	184.62	0.2388	11.96	12.10	0.6638
167858371	rs3822660	T/G	M734I	0.2843	178.01	180.98	0.2553	11.93	12.02	0.6001
167858372	rs3822659	G/T	S735A	0.2843	178.01	180.98	0.2553	11.93	12.02	0.6001
167881030	rs111457550	-/GGA	E965del	2.4000	181.64	178.26	0.2539	11.96	11.97	0.9530
167891750	rs201199684	T/C	S984L	0.0007	179.06	140.89	0.2453	11.97	10.11	0.3821
167891764	rs147393968	T/C	R989C	0.0011	179.06	156.01	0.3905	11.97	11.41	0.7485

m/M, minor allele/major allele; AAS, Amino Acid Substitution; MAF, Minor Allele Frequency
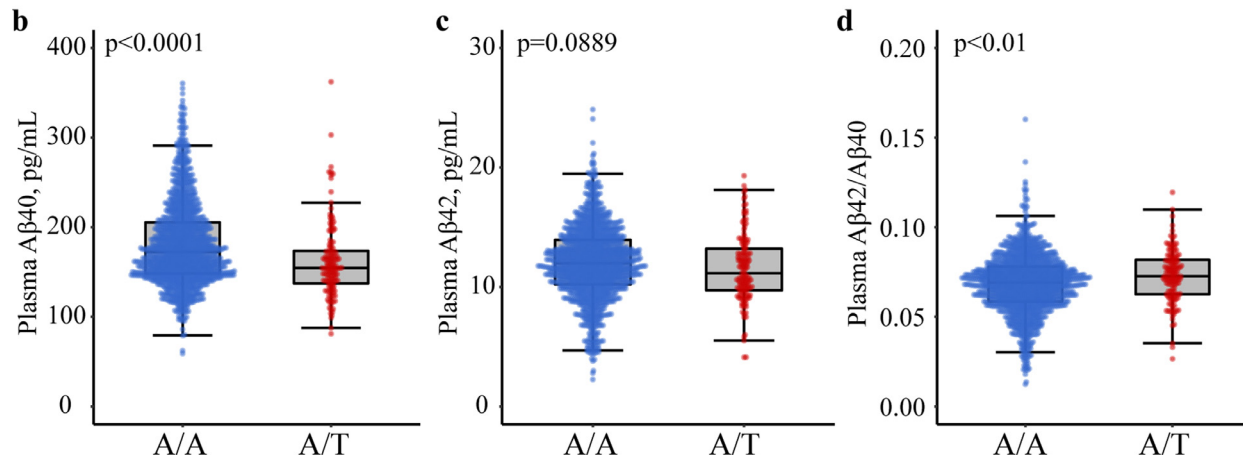
Figure 7. KIBRA genotype effect on plasma Aβ in humans. (**a**) Comparison of plasma Aβ between KIBRA SNPs carriers and non-carriers (n = 1419). P value was calculated by linear regression analysis. (**b-c**) Human plasma Aβ40 (**b**), Aβ42 (**c**), and Aβ42/Aβ40 ratio (**d**) measured by Simoa analysis from subjects with T allele carrier of rs28421695 (A/T) and subjects with A allele carrier of rs28421695 (A/A). All P value was calculated by two-tailed student's t test.

EVs induced the aggregation of the amyloidogenic protein PMEL into PMEL amyloid fibers,[54] which is in a similar manner with formation of Aβ fibers. We found that only a small fraction of Aβ is released in association with EVs (data not shown), and thus, most of the Aβ peptide is released in a free form, which has the potential to associate with EVs extracellularly.[53,55] On the other hand, EVs seem to have the ability to reduce brain Aβ through microglial uptake, and they are known to transfer neuroprotective substances between cells.[56,57]

Our study also evidently show that the stable expression of intracellular APP/Aβ could attribute to the explanation that excessively accumulated MVBs harboring APP-CTFβ/Aβ in KIBRA depletion could be trafficked to lysosomes for amyloid degradation. Previous research has demonstrated that KIBRA is involved in endocytic recycling compartment transport by the SNX4-KIBRA-dynein complex[58] and its C2 domain could bind with PI3P,[16] which is enriched in endosomal membranes. Although findings from the current study indicates that KIBRA regulates transport in subcellular compartments, which part of endo-lysosomal system is primarily affected by KIBRA, as a ligand protein, remains unclear. Endolysosomal dysfunction promotes the release of EVs, while inhibiting EVs secretion inversely promotes the MVB-lysosome fusion, which is a complex process involving many transport molecules.[6] Our current study reveals that KIBRA depletion reduces Rab27a expression in 5XFAD mice and overexpression Rab27a increased the secretion of EVs-associated APP-CTFβ/Aβ (Supplementary Fig. 11), indicating that KIBRA depletion reduces secretion of EVs-associated APP-CTFβ/Aβ mainly by down-regulation of Rab27a protein, which is in line with our previous research.[18] Accumulating evidence suggests that the impairment of endosomal-lysosomal compartments is associated with neurodegenerative disease.[59] In turn, the dysfunction of degradative compartments could trigger the release of EVs, which may spread toxic aggregates in the brain.[34] In our current study, inhibiting lysosomal function by BafA1 and siRab7 has shown to induce a partial rescue of EVs secretion and these approaches can also lead to other endo-lysosomal defects than the simple inhibition of MVB/lysosome fusion. In addition, previous research has shown that Rab7 depletion resulted in large endosomes, filled with ILVs.[24] Therefore, the accumulation of enlarged late endocytic compartments might compensatorily increase the exosome release. In addition, Rab7 depletion could reduce exosomes secretion, which might be explained by the fact that different cells and the different culture times prior to collection of exosomes might have different effects from Rab7 depletion. Therefore, KIBRA regulates amyloid metabolism through interplaying with the balance between subcellular compartments.

Finally, an important question is whether Aβ peptides in MVBs are transported to lysosomes and degraded to non-toxic form. Compared to other endosomal compartments, APP has been found to be enriched in the lysosomes in neuronal cells and is rapidly and directly transported to the lysosomal compartment,[60] which is also observed in our study. A previous study revealed that the lysosome was the major organelle for the production and degradation of Aβ, as well as its fibrillogenesis. However, a recent study demonstrated that late endosomes/lysosomes, where PSEN2/γ-secretase were located in, account for the main pool of the intracellular Aβ.[43]

Etiologically, AD is a multifactorial disease that involves complex interactions of lifelong environmental and genetic factors. Human KIBRA gene is located at the 5q34 locus, and accumulating evidence indicates that KIBRA polymorphism is associated with poor performance in episodic memory as well as increased risk of AD.[9] Previous study identified that two common missense SNPs (rs3822660 and rs3822659) encode variants of the KIBRA C2 domain with the different lipid-binding specificities to affect cognitive performance.[16] Here, our results further indicate that carriers of the KIBRA SNP rs28421695 E862V variant have a lower level of plasma Aβ, which demonstrates the T allele of rs28421695 might exert a protective effect and might be associated with a reduced risk of AD, similar to the carriers of SORL1 SNP rs1784933.[61] However, we did not observe the significant protective effect of rs28421695 against AD in the MIND-China study (Supplementary Table 1), partly due to the limited statistical power. Further investigation is required to tease out the detailed functional significance of this multifunctional protein and consequently its implications for molecular mechanisms of learning and memory and organ size control.

In conclusion, our data explicitly confirm previous report that KIBRA controls EVs secretion, and further show that KIBRA depletion significantly ameliorates extracellular Aβ deposits at the early stage of the disease in the 5XFAD mouse. We further demonstrate that KIBRA controls secretion of EVs-associated APP-CTFβ/Aβ, which subsequently increases the excessive MVB-lysosome fusion for amyloid degradation. Therefore, partially reducing KIBRA levels or activity could be a potential strategy to interfere with multiple AD pathogenic processes and preserve synaptic function in the early stage of the disease.

Contributors
Y.D. and Y.W. designed the study. X.H., C.W., L.S., X. W., S.T., T.H., C.L., and X.L. performed the experiments and analyzed data. Y.W. and Y.D. contributed to

the materials for the study. X.H. wrote the manuscript. X.H., C.W., and Y.W. has directly accessed and verified the underlying data reported in the manuscript. C.Q. has contributed to manuscript preparation and editing. Y.W. and Y.D. were responsible for the decision to submit the manuscript. All authors read, critically revised, and approved the final version of the manuscript.

Data sharing statement

The datasets used and/or analyzed during the current study are available from the corresponding author upon reasonable request.

Declaration of interests

The authors declare no financial or other conflicts of interest.

Supplementary materials

Supplementary material associated with this article can be found in the online version at doi:10.1016/j.ebiom.2022.103980.

References

1 Goedert MSS, Price DL. Neurofibrillary tangles and beta-amyloid deposits in Alzheimer's disease. *Curr Opin Neurobiol*. 1991;1 (3):441–447.
2 van der Kant R, Goldstein LS. Cellular functions of the amyloid precursor protein from development to dementia. *Dev Cell*. 2015;32 (4):502–515.
3 Honig LS, Vellas B, Woodward M, et al. Trial of solanezumab for mild dementia due to Alzheimer's disease. *N Engl J Med*. 2018;378 (4):321–330.
4 Egan MF, Kost J, Tariot PN, et al. Randomized trial of verubecestat for mild-to-moderate Alzheimer's disease. *N Engl J Med*. 2018;378 (18):1691–1703.
5 Salloway S, Sperling R, Fox NC, et al. Two phase 3 trials of bapineuzumab in mild-to-moderate Alzheimer's disease. *N Engl J Med*. 2014;370(4):322–333.
6 Becot A, Volgers C, van Niel G. Transmissible endosomal intoxication: a balance between exosomes and lysosomes at the basis of intercellular amyloid propagation. *Biomedicines*. 2020;8(8):272.
7 Arbo BD, Cechinel LR, Palazzo RP, Siqueira IR. Endosomal dysfunction impacts extracellular vesicle release: central role in Aβ pathology. *Ageing Res Rev*. 2020;58:101006.
8 Swaminathan GZW, Plowey ED. BECN1/beclin 1 sorts cell-surface APP/amyloid β precursor protein for lysosomal degradation. *Autophagy*. 2016;12(12):2404–2419.
9 Papassotiropoulos ASD, Huentelman MJ, Hoerndli FJ, et al. Common KIBRA alleles are associated with human memory performance. *Science*. 2006;314(5798):475–478.
10 Zhang L, Yang S, Wennmann DO, Chen Y, Kremerskothen J, Dong J. KIBRA: in the brain and beyond. *Cell Signal*. 2014;26 (7):1392–1399.
11 Makuch L, Volk L, Anggono V, et al. Regulation of AMPA receptor function by the human memory-associated gene KIBRA. *Neuron*. 2011;71(6):1022–1029.
12 Duning KSE, Schlüter M, Bayer M, et al. KIBRA modulates directional migration of podocytes. *J Am Soc Nephrol*. 2008;19 (10):1891–1903.
13 Kremerskothen JPC, Büther K, Finger I, et al. Characterization of KIBRA, a novel WW domain-containing protein. *Biochem Biophys Res Commun*. 2003;300(4):862–867.
14 Vogt-Eisele AKC, Duning K, Weber D, et al. KIBRA (KIdney/ BRAin protein) regulates learning and memory and stabilizes protein kinase Mζ. *J Neurochem*. 2014;128(5):686–700.
15 Ji Z, Li H, Yang Z, et al. KIBRA modulates learning and memory via binding to dendrin. *Cell Rep*. 2019;26(8):2064–2077.e7.
16 Duning KWD, Bokemeyer A, Reissner C, et al. Common exonic missense variants in the C2 domain of the human KIBRA protein modify lipid binding and cognitive performance. *Transl Psychiatry*. 2013;3:6.
17 Morel E, Chamoun Z, Lasiecka ZM, et al. Phosphatidylinositol-3-phosphate regulates sorting and processing of amyloid precursor protein through the endosomal system. *Nat Commun*. 2013;4:2250.
18 Song L, Tang S, Han X, et al. KIBRA controls exosome secretion via inhibiting the proteasomal degradation of Rab27a. *Nat Commun*. 2019;10(1):1639.
19 Han X, Jiang Z, Li Y, et al. Sex disparities in cardiovascular health metrics among rural-dwelling older adults in China: a population-based study. *BMC Geriatr*. 2021;21(1):158.
20 Théry C, AS RG, Clayton A. Isolation and characterization of exosomes from cell culture supernatants and biological fluids. *Curr Protoc Cell Biol*. 2006;Chapter 3:Unit 3.22.
21 Thery C, Witwer KW, Aikawa E, et al. Minimal information for studies of extracellular vesicles 2018 (MISEV2018): a position statement of the international society for extracellular vesicles and update of the MISEV2014 guidelines. *J Extracell Vesicles*. 2018;7:(1) 1535750.
22 Vella LJ, Scicluna BJ, Cheng L, et al. A rigorous method to enrich for exosomes from brain tissue. *J Extracell Vesicles*. 2017;6:(1) 1348885.
23 de Wolf F, Ghanbari M, Licher S, et al. Plasma tau, neurofilament light chain and amyloid-β levels and risk of dementia; a population-based cohort study. *Brain*. 2020;143(4):1220–1232.
24 Bachurski D, Schuldner M, Nguyen PH, et al. Extracellular vesicle measurements with nanoparticle tracking analysis - an accuracy and repeatability comparison between NanoSight NS300 and Zeta-View. *J Extracell Vesicles*. 2019;8:(1) 1596016.
25 Vorhees CVWM. Morris water maze: procedures for assessing spatial and related forms of learning and memory. *Nat Protoc*. 2006;1 (2):848–858.
26 Kivipelto M, Mangialasche F, Snyder HM, et al. World-Wide FINGERS Network: a global approach to risk reduction and prevention of dementia. *Alzheimers Dement*. 2020;16(7):1078–1094. the journal of the Alzheimer's Association.
27 Jack CR, Albert MS, Knopman DS, et al. Introduction to the recommendations from the national institute on aging-Alzheimer's association workgroups on diagnostic guidelines for Alzheimer's disease. *Alzheimers Dement*. 2011;7(3):257–262.
28 Jiang Z, Han X, Wang Y, et al. Red cell distribution width and dementia among rural-dwelling older adults: the MIND-China study. *J Alzheimers Dis*. 2021;83(3):1187–1198.
29 Zhou X, Chen Y, Mok KY, et al. Identification of genetic risk factors in the Chinese population implicates a role of immune system in Alzheimer's disease pathogenesis. *Proc Nat Acad Sci U S A*. 2018;115(8):1697–1706.
30 Arbo BD, Cechinel LR, Palazzo RP, Siqueira IR. Endosomal dysfunction impacts extracellular vesicle release: central role in Abeta pathology. *Ageing Res Rev*. 2020;58:101006.

31 Lee SJNE, Lee HJ, Savelieff MG, Lim MH. Towards an understanding of amyloid-β oligomers: characterization, toxicity mechanisms, and inhibitors. *Chem Soc Rev.* 2017;46(2):310–323.

32 Esquerda-Canals G, Marti-Clua J, Roda AR, Villegas S. An intracellular amyloid-beta/AbetaPP epitope correlates with neurodegeneration in those neuronal populations early involved in Alzheimer's disease. *J Alzheimers Dis.* 2017;59(3):1079–1096.

33 Braulke TBJ. Sorting of lysosomal proteins. *Biochim Biophys Acta.* 2009;1793(4):605–614.

34 Miranda AM, Lasiecka ZM, Xu Y, et al. Neuronal lysosomal dysfunction releases exosomes harboring APP C-terminal fragments and unique lipid signatures. *Nat Commun.* 2018;9(1):291.

35 van Deurs B HP, Sandvig K. Inhibition of the vacuolar H (+)-ATPase with bafilomycin reduces delivery of internalized molecules from mature multivesicular endosomes to lysosomes in HEp-2 cells. *Eur J Cell Biol.* 1996;69(4):343–350.

36 van Weert AW DK, Geuze HJ, Maxfield FR, Stoorvogel W. Transport from late endosomes to lysosomes, but not sorting of integral membrane proteins in endosomes, depends on the vacuolar proton pump. *J Cell Biol.* 1995;130(4):821–834.

37 Vanlandingham PACB. Rab7 regulates late endocytic trafficking downstream of multivesicular body biogenesis and cargo sequestration. *J Biol Chem.* 2009;284(18):12110–12124.

38 Posner MG, Upadhyay A, Ishima R, et al. Distinctive phosphoinositide- and Ca(2+)-binding properties of normal and cognitive performance-linked variant forms of KIBRA C2 domain. *J Biol Chem.* 2018;293(24):9335–9344.

39 Peric A, Annaert W. Early etiology of Alzheimer's disease: tipping the balance toward autophagy or endosomal dysfunction? *Acta Neuropathol.* 2015;129(3):363–381.

40 Willen K, Edgar JR, Hasegawa T, Tanaka N, Futter CE, Gouras GK. Abeta accumulation causes MVB enlargement and is modelled by dominant negative VPS4A. *Mol Neurodegener.* 2017;12(1):61.

41 Rajendran LHM, Zahn TR, Keller P, Geiger KD, Verkade P, Simons K. Alzheimer's disease beta-amyloid peptides are released in association with exosomes. *Proc Natl Acad Sci U S A.* 2006;103 (30):11172–11177.

42 Bellingham SA, Guo BB, Coleman BM, Hill AF. Exosomes: vehicles for the transfer of toxic proteins associated with neurodegenerative diseases? *Front Physiol.* 2012;3:124.

43 Sannerud R, Esselens C, Ejsmont P, et al. Restricted location of PSEN2/gamma-secretase determines substrate specificity and generates an intracellular Abeta pool. *Cell.* 2016;166(1):193–208.

44 Lauritzen I, Pardossi-Piquard R, Bourgeois A, et al. Intraneuronal aggregation of the beta-CTF fragment of APP (C99) induces Abeta-independent lysosomal-autophagic pathology. *Acta Neuropathol.* 2016;132(2):257–276.

45 Ling D, Salvaterra PM. Brain aging and Abeta(1)(-)(4)(2) neurotoxicity converge via deterioration in autophagy-lysosomal system: a conditional Drosophila model linking Alzheimer's neurodegeneration with aging. *Acta Neuropathol.* 2011;121(2):183–191.

46 Song L, Tang S, Dong L, et al. The neuroprotection of KIBRA in promoting neuron survival and against amyloid beta-induced apoptosis. *Front Cell Neurosci.* 2019;13:137.

47 Ngolab J, Trinh I, Rockenstein E, et al. Brain-derived exosomes from dementia with Lewy bodies propagate alpha-synuclein pathology. *Acta Neuropathol Commun.* 2017;5(1):46.

48 Sardar Sinha M, Ansell-Schultz A, Civitelli L, et al. Alzheimer's disease pathology propagation by exosomes containing toxic amyloid-beta oligomers. *Acta Neuropathol.* 2018;136(1):41–56.

49 Guo M, Wang J, Zhao Y, et al. Microglial exosomes facilitate alpha-synuclein transmission in Parkinson's disease. *Brain.* 2020;143 (5):1476–1497.

50 Winston CN, Aulston B, Rockenstein EM, et al. Neuronal exosome-derived human tau is toxic to recipient mouse neurons *in vivo*. *J Alzheimers Dis.* 2019;67(2):541–553.

51 Lim CZJ, Zhang Y, Chen Y, et al. Subtyping of circulating exosome-bound amyloid beta reflects brain plaque deposition. *Nat Commun.* 2019;10(1):1144.

52 Dinkins MB, Dasgupta S, Wang G, Zhu G, Bieberich E. Exosome reduction *in vivo* is associated with lower amyloid plaque load in the 5XFAD mouse model of Alzheimer's disease. *Neurobiol Aging.* 2014;35(8):1792–1800.

53 Dinkins MB, Enasko J, Hernandez C, et al. Neutral sphingomyelinase-2 deficiency ameliorates Alzheimer's disease pathology and improves cognition in the 5XFAD mouse. *J Neurosci.* 2016;36 (33):8653–8667.

54 van Niel G, Bergam P, Di Cicco A, et al. Apolipoprotein E regulates amyloid formation within endosomes of pigment cells. *Cell Rep.* 2015;13(1):43–51.

55 Falker C, Hartmann A, Guett I, et al. Exosomal cellular prion protein drives fibrillization of amyloid beta and counteracts amyloid beta-mediated neurotoxicity. *J Neurochem.* 2016;137(1):88–100.

56 Cui GH, Wu J, Mou FF, et al. Exosomes derived from hypoxia-preconditioned mesenchymal stromal cells ameliorate cognitive decline by rescuing synaptic dysfunction and regulating inflammatory responses in APP/PS1 mice. *FASEB J.* 2018;32(2):654–668.

57 Cai ZY, Xiao M, Quazi SH, Ke ZY. Exosomes: a novel therapeutic target for Alzheimer's disease? *Neural Regen Res.* 2018;13(5):930–935.

58 Traer CJ, Rutherford AC, Palmer KJ, et al. SNX4 coordinates endosomal sorting of TfnR with dynein-mediated transport into the endocytic recycling compartment. *Nat Cell Biol.* 2007;9(12):1370–1380.

59 Malik BRMD, Smith GA, Peters OM. Autophagic and endo-lysosomal dysfunction in neurodegenerative disease. *Mol Brain.* 2019;12(1):100.

60 Lorenzen A, Samosh J, Vandewark K, et al. Rapid and direct transport of cell surface APP to the lysosome defines a novel selective pathway. *Mol Brain.* 2010;3:11.

61 Chou CT, Liao YC, Lee WJ, Wang SJ, Fuh JL. SORL1 gene, plasma biomarkers, and the risk of Alzheimer's disease for the Han Chinese population in Taiwan. *Alzheimers Res Ther.* 2016;8(1):53.